Design of a Molten Salt Flow Cell for Combined Absorbance and Laser-Induced Breakdown Spectroscopy and Online Measurements

Hunter B. Andrews,[1,*] Zechariah B. Kitzhaber,[1] Daniel Orea,[2] Luke R. Sadergaski,[1] Benjamin T. Manard,[3] Kevin Robb,[2] Joanna McFarlane[2]

[1]Radioisotope Science and Technology Division, Oak Ridge National Laboratory, Oak Ridge, Tennessee, USA
[2]Nuclear Energy and Fuel Cycle Division, Oak Ridge National Laboratory, Oak Ridge, Tennessee, USA
[3]Chemical Sciences Division, Oak Ridge National Laboratory, Oak Ridge, Tennessee, USA
*Corresponding author: andrewshb@ornl.gov

For consideration in *Applied Spectroscopy*

Keywords: laser-induced breakdown spectroscopy (LIBS); molten salt; liquid LIBS; flowing salt; absorbance spectroscopy; real-time monitoring; flow cell

Abstract

A novel flow cell allowing for multiple optical spectroscopy measurements on flowing molten salts was designed, and demonstrative calibrations of impurities in aqueous samples were performed. Online compositional measurements of molten salts are of high interest to monitor the state of relevant solar and nuclear systems. The SCORCH (Spectroscopic Configuration for Optical Real-time Characterization of High-temperature fluids) cell was designed to meet this need by providing optical access to a high-temperature molten salt sample stream without physical contact between the sample and window materials. Laser-induced breakdown spectroscopy (LIBS) was utilized to quantify Li, Cr, Fe, Ni, Sr, and Pr at concentrations ranging nominally from 0 to 315 mMol L^{-1}. Laser power, frequency, and plasma position were optimized to mitigate challenges associated with sample splashing. Univariate calibration models were built with $R^2 > 0.98$, percent root mean square error of cross validation (%RMSECV) as low as 2.7%, and limits of quantification (LOQs) down to 4.11 mMol L^{-1}. Simultaneously, absorbance calibrations were developed for the applicable analytes (Cr, Ni, and Pr) using Beer's law with a pathlength of 4.41 ± 0.10 mm. These models provide excellent quantification performance with $R^2 > 0.999$, %RMSECV as low as 0.6%, and LODs down to 0.080 mMol L^{-1}. Although these calibrations were performed for each spectroscopic technique separately, the two methods may be combined in the future through multivariate modeling and sensor fusion to provide more robust models with the benefits of both techniques (e.g., absorbance: oxidation state concentrations, LIBS: elemental concentration). Additionally, optimized spectrometers may be deployed to enhance sensitivity and detection limits.

1. Introduction

Molten salt technology is gaining interest because of the high-temperature fluid's use in concentrated solar power,[1] fusion energy systems,[2] and advanced nuclear fission reactor designs.[3] A molten salt reactor (MSR) is one of the advanced reactor concepts being developed in which the nuclear fuel is dissolved into a liquid salt that circulates through the core. MSRs are gaining interest because of their efficiency benefits, passive safety features, and potential for medical isotope recovery.[3-6] Because of their chemical complexity, online measurements are imperative to monitor the fissile content of the fuel salt,[7] evaluate corrosion,[8-10] and feed digital models of the reactors with benchmark data.[11, 12] However, MSRs are challenging to monitor with traditional analytical instrumentation because of their high-temperature operation, corrosive environment, and high radiation levels at the location of sensors—all characteristics inherent to the MSR's design. Optical spectroscopy has been proposed to monitor the salt composition in situ as an alternative to radiation-based measurements, which are challenging because of high background levels.

Optical spectroscopy offers a remote detection capability using propagated light and fiber optics to measure hazardous, radioactive, and complex materials while keeping sensitive electronic equipment in shielded areas. Absorbance spectroscopy is a useful remote monitoring technique for analyte oxidation state and concentration because of its passive interaction with sample streams; it simply measures the change in transmitted photons when a light source is passed through a sample versus a reference. Absorbance spectroscopy has been explored previously with demonstrations on quantifying U in molten salts[13]. Additionally, measuring light–salt interactions offers insight into the behavior of radiative heat transfer in salts.[14] However, absorbance measurements typically necessitate window materials that contact the salt. This is a challenge for fluoride salts because etching occurs with many transparent materials.[15] Although previous windowless systems have been designed, they have only been demonstrated for static salt samples.[16, 17] Raman spectroscopy can identify molecular species and has been applied to monitoring the liquid salt and cover gas phases.[13, 18] Similar to absorbance measurements, Raman measurements in the liquid salt phase must overcome material compatibility issues. Finally, laser-induced breakdown spectroscopy (LIBS) has been proposed for evaluating the elemental composition of molten salts and has been explored previously with liquid[19-22] and aerosolized salts.[23-25] LIBS is performed by forming a microplasma from ablated sample material and measuring the characteristic optical emissions.[26] LIBS offers a powerful in situ monitoring tool because of its wide sensitivity to nearly all elements.

Because each spectroscopic technique has its own advantages and disadvantages, combined optical measurements using multiple techniques (e.g., LIBS for elemental analysis and Raman for molecular) are especially attractive. The use of combined spectroscopic techniques on liquids has been demonstrated; however, many of these systems would not be suitable with a high temperature molten salt due to window material compatibility with the salts themselves.[27-29] Furthermore, in many cases, the two types of analyses do not occur in the same physical location, which could lead to discrepancies in results because molten salt systems can be highly dynamic. The solution to these issues is a system capable of online, co-located absorbance and LIBS measurements compatible with high-temperature, corrosive molten salts.

LIBS on liquids is challenging because of splashing effects caused by the ablation shockwave, which results in droplets forming on optical components.[30] Direct LIBS analysis of molten salts has been explored several times, but the challenges are only compounded by the high-temperature salt. Many of these experimental setups require a furnace and windows to retain an inert atmosphere (unless performed in a glovebox environment). Additionally, to the best of the authors' knowledge, direct liquid-phase measurements on flowing salt have never been reported. Analyzing aerosolized salts is promising because of the removal of splashing effects and the demonstrated protection

of optical windows using a sheath gas.[31] The main barrier for aerosolized salt measurements is related to transport between aerosol generation and measurement, as well as the dilution of the salt material by the carrier gas.[25] One approach used in literature for aqueous liquid LIBS measurements is through the formation of jets, where the high velocity of the jet results in a repeatable and constantly refreshed sample surface for LIBS measurements, and any splashing is directed away from the optical components.[30] Unfortunately, for molten salts, a jet design similar to that previously reported may not be ideal because of potential clogging concerns related to the small-diameter nozzles.

In this study, a compatible spectroscopy flow cell for online measurements of flowing molten salt was developed and tested on aqueous sample streams as a proof-of-concept with three primary goals: (1) design a flow cell for LIBS and spectrophotometry measurements compatible with the temperatures for molten salts, (2) demonstrate the quantification capabilities of LIBS, and (3) demonstrate the quantification capabilities of absorbance/transmittance spectrophotometry using the proposed design with the flow cell system. The integration of absorbance spectroscopy and LIBS within a single flow cell architecture offers a powerful, multimodal platform for in situ chemical analysis of flowing molten salts. Absorbance enables quantitative tracking of optically active species, including dissolved corrosion products and redox-active components, through their characteristic electronic transitions. LIBS complements this by providing broadband elemental analysis of suspended particulates, precipitates, and transient species that may elude detection via the available optical absorption window. Together, these modalities provide complementary sensitivity to molecular and elemental signatures, which enhances diagnostic coverage and enables robust characterization of corrosion dynamics, impurity transport, and speciation under evolving process conditions. This dual-spectroscopy approach supports improved calibration strategies, facilitates cross validation, and strengthens attribution of chemical signatures in complex, high-temperature environments relevant to nuclear and electrochemical systems. The result of this study is a dual-sensor system prepared for further testing with molten salts to enable online spectroscopy measurements for monitoring flowing salt systems and, ultimately, MSRs.

2. Experimental

Flowing Salt Spectroscopy Cell Design

Borrowing from the current generation of molten salt aerosol LIBS measurement cells,[24] a new flowing liquid-phase molten salt LIBS measurement cell was designed. The cell design is referred to hereafter as the SCORCH (Spectroscopic Configuration for Optical Real-time Characterization of High-temperature fluids) cell. In this design, a liquid column falls (e.g., gravity-driven) through a flanged cube (**Fig. S1**). The sample stream inlet tube's inner diameter is nominally 4.9 mm, which is large enough to mitigate clogging

challenges. The inlet tube is equipped with a concentric sheath gas to surround the column of salt with an inert gas and prevent air exposure. After the sample is passed through the SCORCH cell, it drains to a lower reservoir. In this study, a constant flow rate of 1 L min^{-1} was used to simulate anticipated molten salt flow rates in a planned loop design.

The stainless-steel flanged cube provides optical access to the sample stream from four directions. The front optical access is used for LIBS measurements. The front face of the flanged cube is equipped with a ConFlat flange expander with a fused-silica window (J. Kurt Lesker). The flange expander provides a larger angle of access to the salt stream and separates the window from the sample stream by 75 mm. This distance permits trace heating and insulation for maintaining the temperature of the molten salts being analyzed and mitigates the heat load on the window. The SCORCH cell is made of materials (cube, flanges, gaskets, fasteners) compatible with temperatures up to 800 °C. In the aqueous prototype of the SCORCH cell used in this study, the lower reservoir was used to make additions or dilutions for calibrations. The sample material in the reservoir was pumped vertically into an upper plenum to replenish the falling liquid.

LIBS was performed by firing a nanosecond pulsed laser through a beam expander, a dichroic mirror, and then a focal lens toward the front surface of the liquid stream. In this setup, the beam expander reduces the fluence on the window to mitigate laser damage during operation and results in a tighter focused ablation spot. The plasma emissions are collected collinearly with the same focal lens. The emission light is reflected by the dichroic mirror and focused into a fiber bundle, which is routed to a multichannel spectrometer. Multichannel spectrometers are compact and rugged and provide broadband coverage; however, the sensitivity is less than larger narrowband Czerny–Turner spectrometers. Based on the sensitivity and selectivity desired, the spectrometer can be changed accordingly. The optical pathway opposite the LIBS entrance is fixed with a beam dump for any residual laser energy.

The remaining two optical pathways (orthogonal to the LIBS setup) were used for absorbance measurements. In the absorbance setup, each side is outfitted with extension flanges to protect the windows from the heat load and any ejected droplets. A fiber-coupled light source is aligned to pass through the liquid sample stream directly below its inlet into the chamber. This light pathway is above the LIBS focal position, so only low-intensity stray 1064 nm laser light is detected in the absorbance measurement background. Notably, a 1064 nm notch filter could be used if near-infrared (NIR) absorbance is of interest. The collected light is then routed to a compact ultraviolet (UV)–visible (VIS) spectrometer. Although Raman was not explored in this study, the optical pathways to the liquid stream would permit the integration of a Raman probe in a similar manner (i.e., without direct contact between the optics and the sample). A schematic of the SCORCH cell is shown in **Fig. 1**.

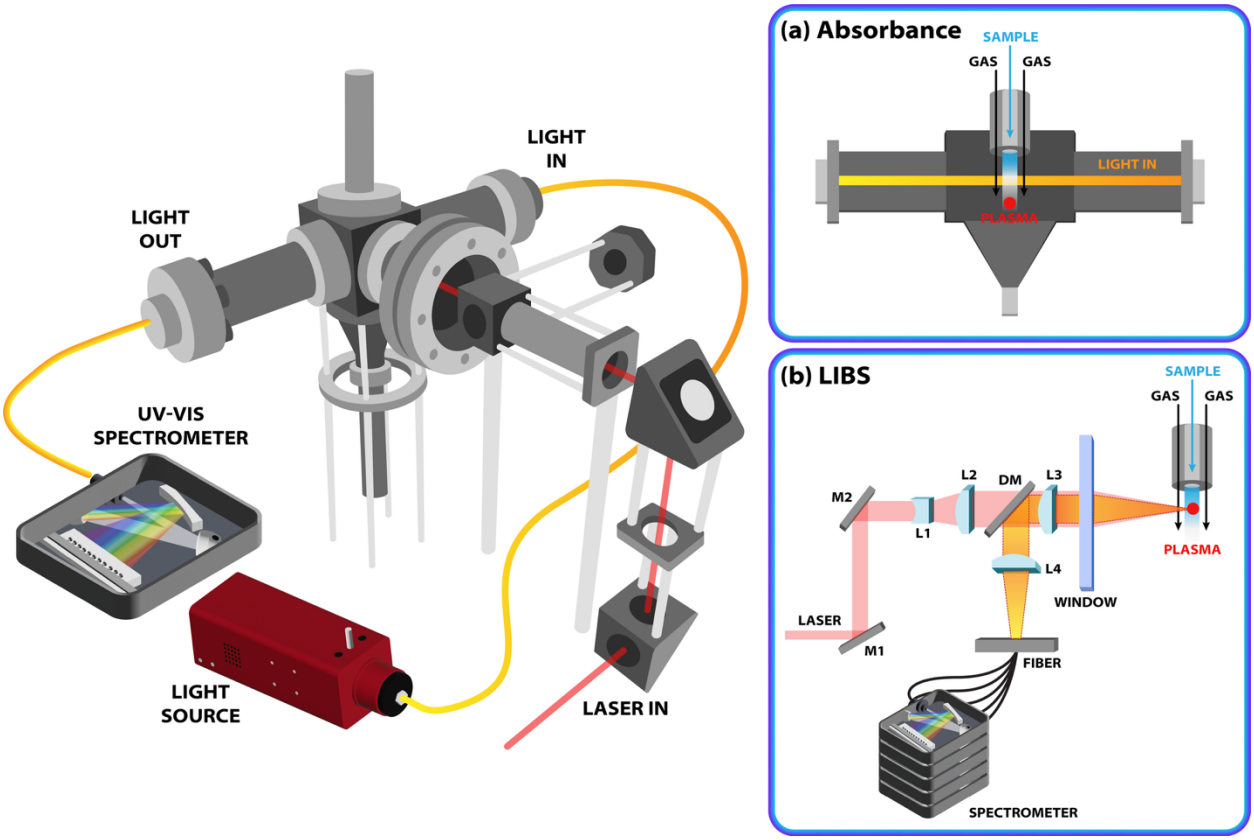

Fig. 1. Schematic of the SCORCH cell design. (a) Sample feedthrough and spectrophotometry measurement approach. (b) LIBS measurement setup (M: mirror, L: lenses, DM: dichroic mirror).

Instrumentation

The laser used for LIBS measurements in this study was a nanosecond pulsed 1064 nm Nd:YAG (Nano, Litron). This laser has a maximum energy of 150 mJ and a maximum frequency of 10 Hz. The LIBS spectrometer used here was a six-channel spectrometer (2048CL, Avantes). The gate delay was set to 0.87 μs, and the integration time was set to 2 ms. The laser energy, shot frequency, and shot accumulation parameters were optimized to maximize analyte signal and minimize splashing effects. The absorbance measurements were obtained using a W–halogen lamp (Thorlabs) and a compact UV–VIS spectrometer (QEPro, Ocean Optics). The light was collimated using FiberPort couplers (Thorlabs) with *X*, *Y*, *Z*, and θ adjustments to pass the lamp light through the sample stream and collect the transmitted light. Sample concentrations were verified using a Thermo Scientific iCAP PRO inductively coupled plasma (ICP)–optical emission spectroscopy instrument.

Samples

Samples were prepared using single-element stock solutions (10,000 µg mL^{-1}, Avantor). The elements investigated in this study were selected to represent species of interest for monitoring in an MSR, including representative bulk salt species (Li, Na), corrosion products (Cr, Fe, Ni), and fission product simulants (Sr, Pr). LIBS and absorbance measurements were taken simultaneously. Analytical samples were taken at each concentration step for analysis to verify concentrations.

Table 1. Calibration concentration ranges.

Element	Concentration Range (mMol L^{-1})
Li	0 – 315
Cr	0 – 45
Ni	0 – 39
Fe	0 – 40
Sr	0 – 27
Pr	0 – 18

Data Analysis, Calibration Modeling, and Statistics

Data analysis was performed using Python 3. For LIBS univariate models, peak areas were calculated using Simpson integration between two selected wavelength values. These peak areas were regressed against concentration. For absorbance univariate models, the absorbance value at a given wavelength was used. At low concentrations relevant to this study, absorbance models are governed by Beer's law (eqn. 1):

$$A_\lambda = \varepsilon_\lambda bc, \#(1)$$

where A_λ is the absorbance at a given wavelength, ε_λ is the molar absorptivity at that wavelength, b is the pathlength, and c is the sample concentration.[32] Absorbance models were regressed by forcing the intercept through zero to match the model to the anticipated Beer's law behavior. Absorbance spectra were baseline-corrected to accommodate this modeling and mitigate any scatter or drift effects.

Calibration models were evaluated based on their coefficient of regression (R^2), which represents the quality of fit, and root mean square error (RMSE), which represents the prediction capabilities. RMSE is defined in eqn. 2 as

$$RMSE = \sqrt{\frac{\sum (y_i - \hat{y}_i)^2}{n}}, \#(2)$$

where y_i is the known concentration, $\hat{y}_i$ is the model-predicted concentration, and n is the total number of samples. The RMSE of calibration (RMSEC) was determined using the predictions of the samples that were used to directly build the model. The RMSE of cross

validation (RMSECV) was determined from the predictions of the samples calculated using the model in which they were not included. Cross validation was performed using a leave-one-group-out approach where each concentration level was withheld from the model construction, and the withheld concentration was predicted by the model built without it. This was iteratively continued until each concentration level was left out of the model once. Because RMSE metrics are in units of concentration, it is often useful to convert RMSE values into percent RMSE (RMSE%) by normalizing the values to the median concentration used in the calibration. In previous online monitoring studies, model efficacy was ranked using RMSE% values, classifying them as strong (RMSE% ≤ 5%), satisfactory (5% < RMSE% ≤ 10%), or indicative (10% < RMSE% ≤ 15%).[33]

For LIBS models the limits of detection (LODs) and limits of quantification (LOQs) were determined using the 95% prediction intervals of the linear model, as described by Mermet.[34] Here, the LOD and LOQ are obtained from the horizontal intersection between the upper prediction band value at a concentration of zero with the fitted regression line and lower prediction band, respectively. The benefit of this approach is that the uncertainty from the entire regression is considered, rather than just the sensitivity factor and variance in the blank signal. Absorbance model LODs and LOQs were determined from the traditional 3σ- and 10σ-methods, respectively. This was done due to Beer's Law dictating the calibrations pass through the origin.

3. Results and Discussion

SCORCH Cell Optimization

The main challenges with measuring molten salts directly with LIBS are splashing and maintaining line of sight through optical windows.[30] The SCORCH cell provides a direct line of sight of the flowing liquid stream. The windows are located a distance away from the molten/liquid sample stream to permit the windows to remain at an operable temperature, and the interior of the cell remains above the melting temperature of the analyte—eventually the salt. This distance also helps mitigate droplets ejected from the liquid stream reaching the windows. Several factors were also optimized in this study to minimize this splashing, including plasma positioning, laser frequency, and laser energy. This work was completed using a solution of nominally 44 mMol L^{-1} Na.

First, the plasma position on the sample stream was optimized. Initially, the plasma was positioned on the center of the liquid, facing the LIBS window. The optics were aligned on a translation stage such that the plasma position could be incrementally varied across the sample stream. The plasma position experiment is illustrated in **Fig. S2**. **Fig. 2** shows the change in LIBS spectra with plasma position. When the plasma was positioned at the sides/edges of the liquid, ablation primarily occurred in the air adjacent to the column, and plasma emissions from gas-phase analytes such as N increased relative to sample species. When the plasma was centered on the sample stream, ablation occurred

primarily in the liquid. The sample signals were maximized, and gas signals were minimized. This also maximized the analyte's signal-to-noise ratio (SNR), defined as an analyte's peak area relative to the root mean square noise in a nearby region, as shown in **Fig. 2**. However, at this position, the splashing was substantial, and droplets were observed impacting the window. Based on this observation, a position of 1 mm to the right of the center was selected. This position slightly decreased the SNR but also sufficiently reduced splashing and eliminated the observed droplets on the window.

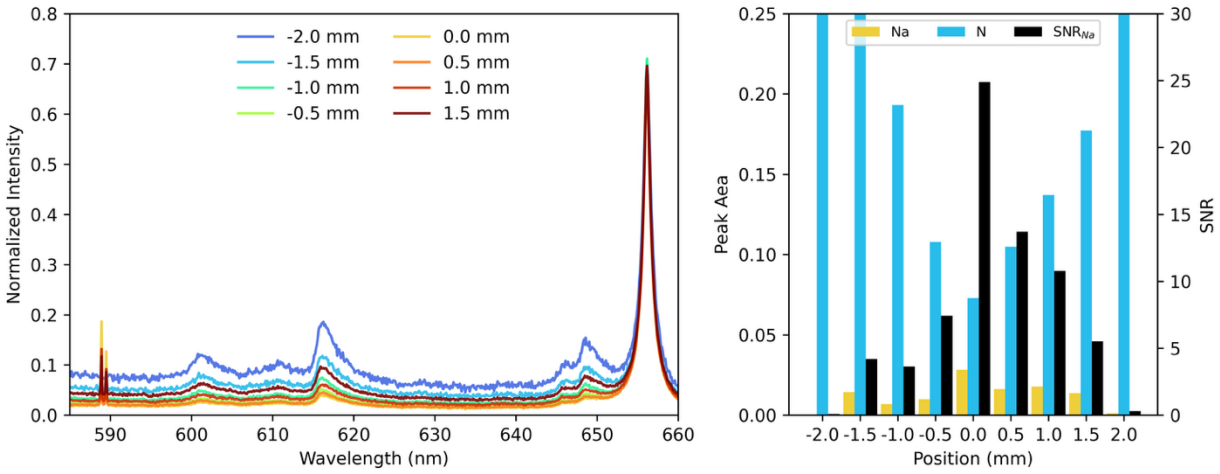

Fig. 2. Optimization of plasma position. (left) LIBS spectra (normalized to H_α 656.27 nm) measured at varying positions across liquid column, and (right) comparison of the sample and atmosphere peak areas versus position, as well as the Na SNR. The position of 0 mm corresponds nominally to the center of the liquid column, facing the LIBS laser optical access.

Next, the laser frequency and energy were explored. High laser frequencies (e.g., 10 Hz) can be beneficial for collecting a greater number of replicates in less time, but the reduced time between shots was found to drastically increase splashing. Lower frequencies (e.g., 1–2 Hz) minimized splashing. The transients of interest in online monitoring of molten salts occur on the order of hours to days, so this reduction in time resolution would have a minimal effect for the intended application. The laser frequency had little to no effect on the quality of the spectra collected other than splashing.

Laser energy typically has a large effect on the quality of LIBS spectra. This study found that lower energy resulted in a higher Na/N ratio (**Fig. 3**). However, an unexpected benefit of higher laser energies was that splashing was drastically reduced. Greater laser energy should result in more efficient atomization of the liquid, including the ejected droplets, thereby preventing them from reaching the windows. However, further studies are required to verify the underlying mechanisms. Based on this result, 150 mJ was used for

the remainder of the study to reduce splashing. Future molten salt experiments will require reoptimizing these parameters because the liquid properties will differ from water.

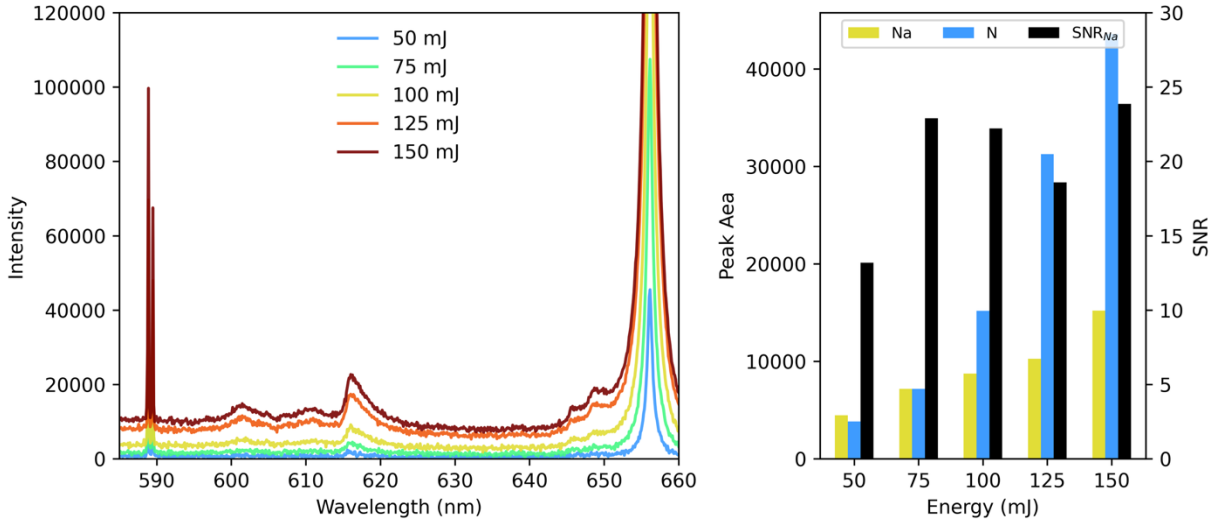

Fig. 3. Optimization of laser energy. (left) LIBS spectra measured at varying energies, and (right) comparison of the sample and atmosphere peak areas, as well as the Na SNR, versus energy. The optimal energy was determined to be 150 mJ because of the reduced splashing effects. Similar SNR performance was measured using 75 mJ, but the splashing was minimized at 150 mJ.

LIBS Detection Capabilities

Several elements, including Li, Sr, Pr, Cr, Ni, and Fe, were selected for a calibration demonstration to highlight the versatility of liquid LIBS measurements for monitoring flowing chemical systems. A calibration for each species was made by spiking the recirculating water in the cell with concentrated ICP standards to increase the concentration stepwise. This concentration range was selected to focus on detecting trace species in solution by assessing detection limits and precision capabilities for quantification. The spectra for the highest-concentrated samples from the calibrations are overlaid with one another in **Fig. 4**, with peaks of interest labeled accordingly. Notably, the dichroic mirror used in emission light collection had a reflection band of 350–1000 nm, and the reflection spectrum of the dichroic contributed significantly to the shape of the background in the 350–600 nm region.

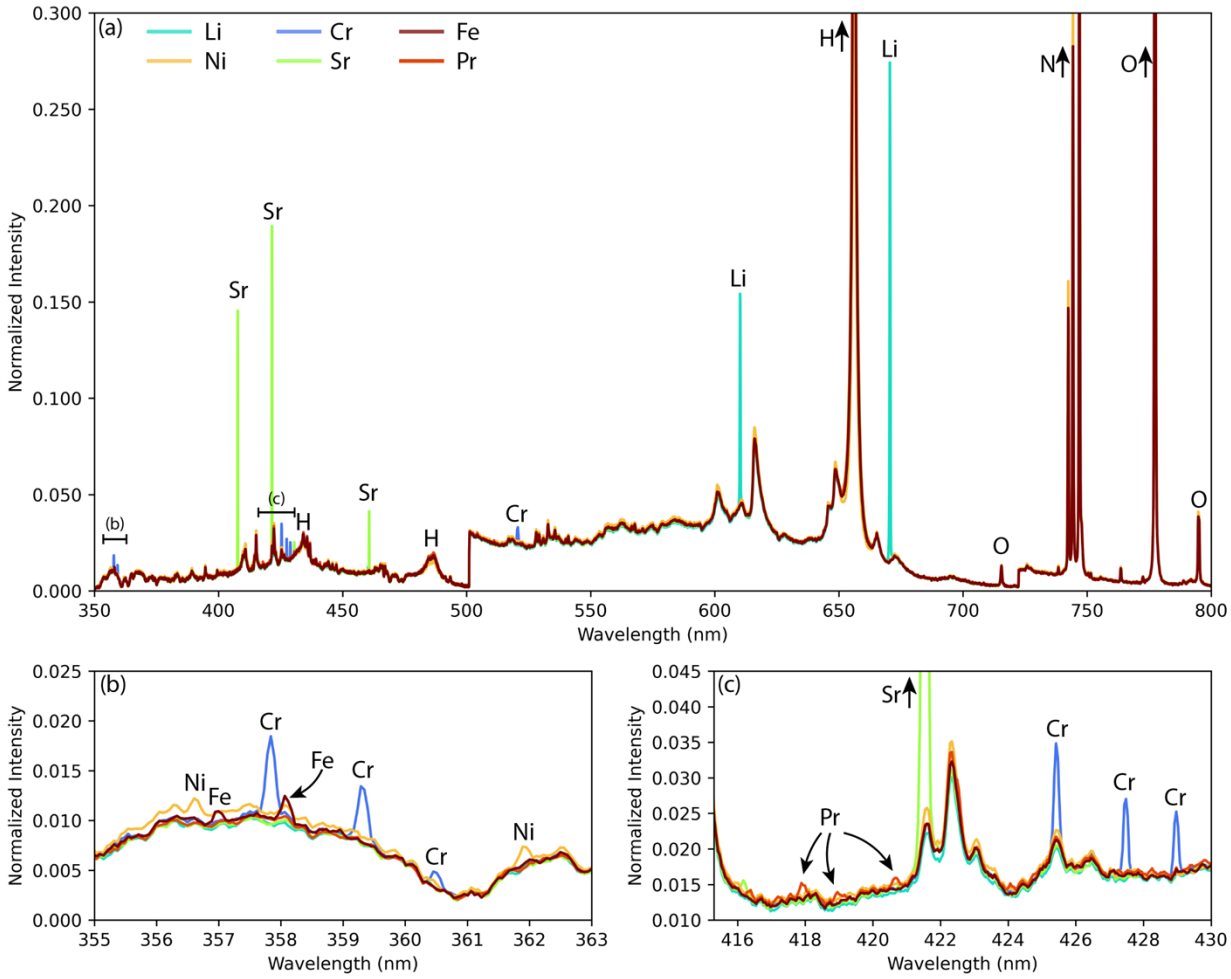

Fig. 4. LIBS spectra of samples containing the highest calibration concentration of each analyte. (a) Broad spectral coverage of the multichannel spectrometer. (b) and (c) Highlighted regions containing less-intense peaks of interest.

The spectra are largely dominated by the bulk elements and atmospheric elements (H, O, N). The alkali metal and alkaline earth metal elements (Li and Sr) provide strong emission peaks because of their electronic structure. The transition metals have a variety of emission intensities. Neutral Cr provides several peaks between 357 and 361 nm, between 424 and 430 nm, and at 520 nm. Cr is a dominant signature of corrosion in molten salts; thus, its detection capabilities are of high interest. Fe and Ni show weaker emission peaks between 356 and 400 nm. The strongest emission peaks for Fe and Ni are 358.12 and 361.94 nm, respectively. Finally, Pr was selected as a representative lanthanide fission product, and it has the weakest emission out of the analytes in this study. Several emission peaks were identified between 415 and 445 nm, with the strongest emission peak at 417.94 nm.

The strongest emission peaks for each element were investigated for use in univariate calibration models. Given the low signal levels for many elements, the average spectra from 500 shots were used for each data point to reduce the noise amplitude; this method corresponds to a measurement time of 4.17 min per spectra. As mentioned previously, the transient nature of most molten salt systems is expected to be far slower than this time, indicating this method uses a sufficient data rate for real-time monitoring. This study found that normalizing spectra to the dominant H_α 656.27 nm peak area improved the figures of merit for all calibration models. Finally, an asymmetric least squares regression ($\lambda = 1 \times 10^5$, $p = 0.005$) was used for baseline correction of all spectra. The optimal LIBS calibration model for each element is shown in **Fig. 5**. Additionally, the figures of merit for each model are provided in **Table 2**.

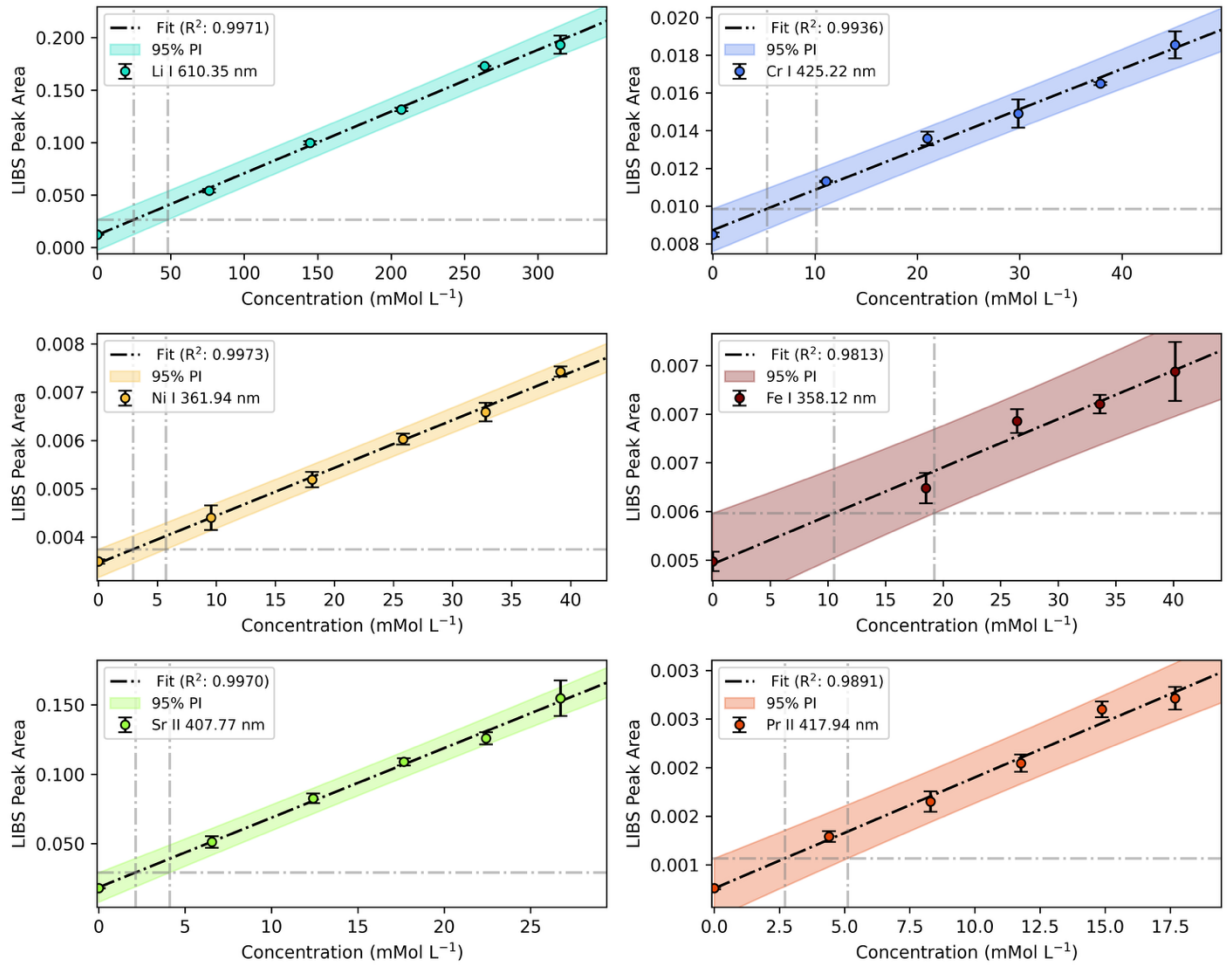

Fig. 5. The optimal LIBS calibration model for each element with 95% prediction intervals. The dashed lines represent how the LODs/LOQs were determined where the first vertical line is the LOD and the second is the LOQ. Note that error bars are the standard deviation of the measured peak areas.

Table 2. LIBS calibration model figures of merit.

	Li I 610.35 nm	Cr I 425.22 nm	Ni I 361.94 nm	Fe I 358.12 nm	Sr II 407.77 nm	Pr II 417.94 nm
R^2	0.9971	0.9936	0.9973	0.9813	0.9970	0.9891
RMSEC (mmol L^{-1})	5.83	1.24	0.69	1.92	0.50	0.63
RMSECV (mmol L^{-1})	8.93	1.95	1.17	2.69	0.73	0.94
%RMSEC	1.9%	2.8%	1.8%	4.8%	1.9%	3.5%
%RMSECV	2.8%	4.3%	3.0%	6.7%	2.7%	5.2%
LOD (mmol L^{-1})	24.9	5.30	2.96	10.5	2.12	2.71
LOQ (mmol L^{-1})	48.1	10.1	5.73	19.2	4.11	5.12

The Li 610.35 nm and Sr 407.77 nm emission peaks were found to provide the two of the best calibration models despite not being the strongest intensity peaks for each element. The Li 670.77 nm peak was not used because of exhibiting signs of self-absorption. The Sr 421.55 nm line was not used because of a slight background interference (as shown in **Fig. 4**). The calibration models for all resulted in strong linear fits (R^2 > 0.98).

The percent RMSE values for calibration and cross validation were calculated to assess the quantification capabilities for each species. The %RMSEC values for all models fell below 5% indicating strong prediction performance. The %RMSECV values represent how well an unknown sample may be quantified. Here, the %RMSECV values increase for each model compared with the %RMSEC values; this result was expected with only five to six calibration points used in the model. Still, nearly all the models still offer strong predictive performance, but the Fe model falls into the satisfactory range. A parity plot of predicted concentrations versus known concentrations for the LIBS models during cross validation is shown in **Fig. S3**.

Finally, LODs and LOQs for each element were estimated by assessing the prediction bands for each model. Although LODs are frequently cited in literature, this discussion focuses on LOQs because they are more pertinent to online monitoring applications. Sr, Pr, and Ni resulted in the lowest LOQs: <10 mMol L^{-1}. The measurement of Sr as a fission product in this concentration regime could be useful for evaluating the burnup of nuclear-fueled molten salts. The LOQ for Pr demonstrates the feasibility of monitoring lanthanide fission products as well. The low LOQ for Ni, followed by the slightly higher LOQ for Cr, indicate the real-time LIBS would be useful for monitoring corrosion products in the salt. The Fe LOQ was estimated to be much greater than the other transition metals. This result is accredited to the stronger Fe LIBS emissions being in the UV region, where signal was lost because of the dichroic mirror's reflective profile. However, future studies could explore alternative light collection schemes or more sensitive spectrometers to

enhance these figures of merit. The elevated LOD for Li may be attributed to its calibration range being far larger than the other analytes (due to its low molar mass). However, detection of trace Li is likely not needed as it would be present as a bulk salt species.

Ultimately, these calibrations prove the feasibility of using LIBS with the SCORCH cell setup to monitor liquid streams in situ. Because these demonstrative tests were completed in water matrices, several factors are anticipated to differ when molten salts are used (e.g., splashing, laser-salt coupling, plasma matrix effects). Future iterations should explore alternative light collection strategies; the dichroic mirror simplifies the experimental setup but results in reduced reflectance below 550 nm and negligible reflectance below 350 nm, providing an upper bound to the wavelength detection region. For many transition metals, UV emissions are dominant; thus, a direct collection of plasma emissions would be expected to enhance the sensitivity of LIBS in the SCORCH cell. Additionally, although these calibrations were performed with a multichannel spectrometer, future studies could investigate a more sensitive setup using sensitive detectors (e.g., an intensified charge-coupled device [ICCD]) and higher-resolution spectrographs to enhance performance.

UV–VIS Spectrophotometry Detection Capabilities

The SCORCH cell was designed to integrate multiple spectroscopic measurements into a single sampling point. During the LIBS calibrations, UV–VIS absorbance measurements were collected simultaneously. Although LIBS is sensitive to nearly all elements, UV–VIS absorbance measurement relies on the strength of the electronic transition. Absorbance measurements are governed by Beer's law (eqn. 1), which relates absorbed light to pathlength and molar absorptivity. Because absorbance measurements are normalized to the intensity of transmitted light in the absence of an analyte, the measurement sensitivity is limited by the dynamic range of the detector that is used.

Cr, Fe, Ni, and Pr can be measured by absorbance, whereas Li and Sr do not absorb light in the UV–VIS range. Fe has a very high molar absorptivity coefficient in the UV range; however, the spectrometer and lamp that were used limited the absorbance window to 400–1000 nm. Cr, Ni, and Pr were successfully measured with a 200 ms exposure time, and each spectrum was the average of 25 measurements, resulting in a 5 s response time for each absorbance measurement. To reduce noise in the absorbance signals, the spectra were smoothed using a 10-point window, first-order Savitzky–Golay filter and were baseline-corrected. The Cr^{3+} absorbance profile provides the strongest signature, with absorbance values more than seven times that of Ni^{2+} and Pr^{3+}. Both Cr^{3+} and Ni^{2+} profiles exhibit broad absorbance bands, which could complicate analysis of mixed systems. Pr^{3+} provides far narrower absorbance bands compared with the transition metals, as is typical of many lanthanides. The absorbance profiles of these elements are shown in **Fig. 6**.

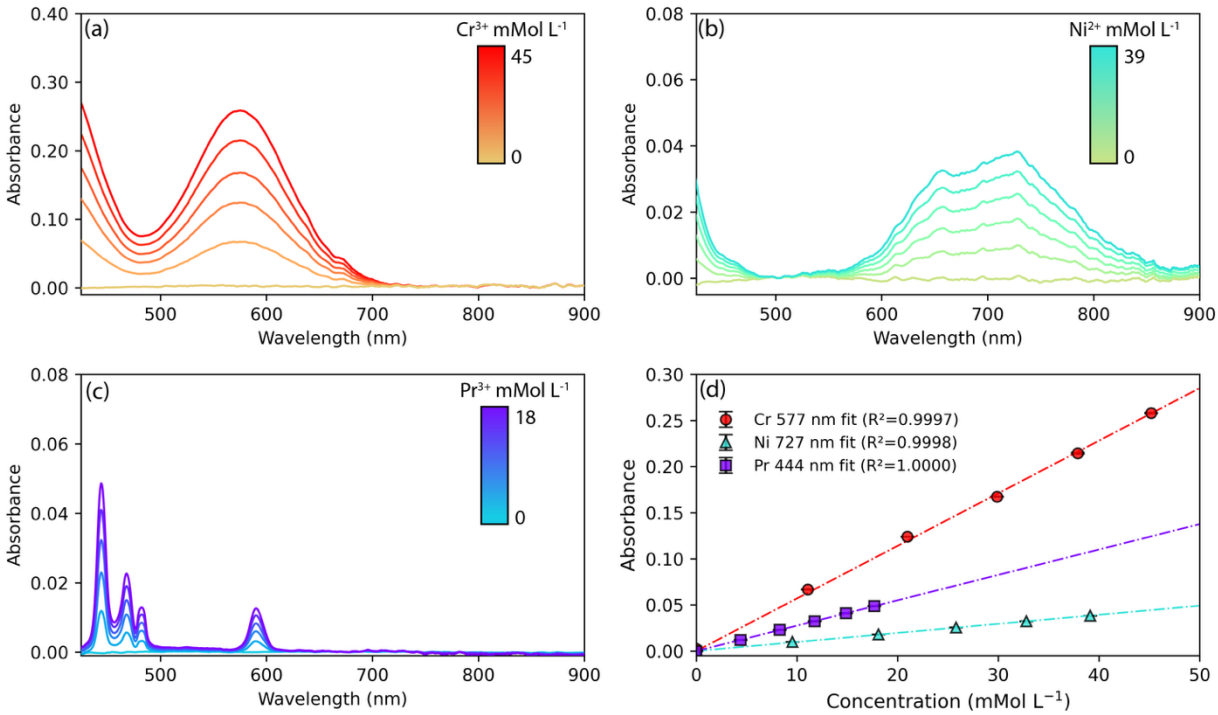

Fig. 6. Absorbance spectra of the (a) Cr^{3+}, (b) Ni^{2+}, and (c) Pr^{3+}. (d) The resultant calibration models governed by Beer's law.

Because the free surface of the sample stream fell through the SCORCH cell, the absorbance pathlength was initially estimated to be the internal diameter of the inlet tube. However, the curvature of the liquid, potential scattering effects, and constriction of the sample stream in free fall affect the effective pathlength. Fortunately, because Beer's law applied, the pathlength of the SCORCH cell was determined by comparing the slope of the absorbance calibrations measured on the cell with those measured with a known pathlength. The grab samples taken at each concentration were measured in a 10 mm cuvette, and the effective pathlength for the SCORCH cell was calculated to be 4.41 ± 0.10 mm using the average of all three analytes. Beyond determining pathlength, this comparison between cuvette measurements and those in the SCORCH cell demonstrated that ex situ absorbance calibrations would be possible when Beer's law is applicable. Beyond Beer's law, multivariate modeling can be used to quantify analytes when nonlinear effects occur, such as temperature-based peak shifts, solute–solute interactions, and the overlap of multiple analyte absorbance bands.

The univariate models for absorbance measurements are shown in **Fig. 6(d)**. The figures of merit for these models are provided in **Table 3**. The calibrations provided very strong fits, with all R^2 values greater than 0.999. As with the LIBS calibrations, the %RMSE values for calibration and cross validation were calculated to assess the quantification capabilities for each species. All %RMSEC values fell below 5%, indicating a strong

prediction performance. A cross validation was performed to investigate performance when samples were not included in the calibration, yielding an excellent prediction accuracy for all analytes. A parity plot of predicted concentrations versus known concentrations for the absorbance models during cross validation is shown in **Fig. S4**.

When compared with the LIBS calibration models, the absorbance models offer between a 1.6 – 8.4× improvement prediction performance, based on their reduction in %RMSECV. The LOQ for the absorbance models is also significantly lower than their LIBS counterparts. The increased sensitivity for Cr^{3+} would be particularly beneficial for early detection of corrosion. Future iterations of the SCORCH cell could incorporate a mirror to double the pathlength of the transmitted light and effectively halve the LOQs.

Table 3. Absorbance calibration model figures of merit.

	Cr^{3+} 577 nm	Ni^{2+} 727 nm	Pr^{3+} 444 nm
R^2	0.9997	0.9998	1.0000
RMSEC (mmol L^{-1})	0.501	0.325	0.053
RMSECV (mmol L^{-1})	0.556	0.354	0.056
%RMSEC	2.2%	1.7%	0.6%
%RMSECV	2.5%	1.8%	0.6%
LOD (mmol L^{-1})	0.080	0.397	0.209
LOQ (mmol L^{-1})	0.264	1.31	0.690

4. Conclusions

Monitoring impurities in molten salt systems as they are used in flowing systems for concentrated solar power, MSRs, and fusion reactor blankets is a largely unmet need. Although LIBS has been under development for monitoring aerosolized salt or off-gas systems, its application to direct liquid salt measurements has been challenging because of issues related to the interaction between the laser-induced plasma shockwave and the liquid itself (e.g., splashing). Additionally, LIBS measurements of flowing molten salts have not been demonstrated. Although other optical spectroscopy methods have been applied directly to salts, they are challenging because of material compatibility issues related to the etching of optical windows. In the present study, the SCORCH cell offers a novel approach to incorporate multiple optical techniques without direct contact between flowing molten salts and windows and to alleviate challenges of LIBS on liquids. The combination of LIBS and absorbance spectroscopy within a single flow cell design offers a powerful, multimodal platform for in situ chemical analysis for flowing molten salts. This dual-spectroscopy approach supports improved calibration strategies, facilitates cross validation, and strengthens attribution of chemical signatures in complex, high-temperature environments relevant to nuclear and electrochemical systems.

The utility of the SCORCH cell was demonstrated through the calibration of several relevant elements in aqueous solutions using both LIBS and absorbance measurements. Successful LIBS calibrations for Li, Cr, Ni, Fe, Sr, and Pr were constructed, with LOQs as low as 4 mMol L^{-1} and %RMSECV values as low as 2.7%. Similarly, absorbance calibrations for Cr^{3+}, Ni^{2+}, and Pr^{3+} were successfully developed. The calibrations followed Beer's law, with LOQs as low as 0.264 mMol L^{-1} and %RMSECV values as low as 0.6%. Additionally, the capability to perform ex situ absorbance calibrations was shown to be possible.

These calibrations demonstrated the complementary nature of LIBS and absorbance. Although LIBS offers broader coverage of multiple analytes, absorbance can be more sensitive for select analytes. Additionally, although absorbance spectra exhibit broad signatures, LIBS emission peaks are narrow, and generally, multiple are present for a given analyte. The complementary methods support a sensor fusion approach in which the spectra or extracted features from each technique are regressed in a single multivariate model.[27, 28] For example, Beer's law fails at high optical density; thus, the presence of multiple absorbing species and entrained particulates could limit the dynamic range of an absorbance spectrometer. However, as the concentration of species increases, additional LIBS emission peaks grow in, and quantification will still be feasible. This is the power and benefit of tandem optical spectroscopy techniques.

The next step in this work will be the construction of a high-temperature molten salt system in which the SCORCH cell capabilities can be tested. The LIBS parameters used to reduce splashing (e.g., focal position/depth, laser energy, repetition rate) will likely change because of the changes in the liquid properties. Other enhancements to the measurement system, such as improved spectrometers (e.g., higher resolution, ICCD cameras) and different light sources (e.g., UV or NIR), may also be investigated to meet required levels of sensitivity.

Data Availability

All relevant data that support these experimental findings are available from the corresponding author upon reasonable request.

Acknowledgments

The authors would like to acknowledge Jacquelyn Demink for assistance with graphics. This work was funded by the US Department of Energy's Office of Nuclear Energy, Advanced Reactor Development Program, Molten Salt Reactor Program. This research was supported by the US Department of Energy Isotope Program, managed by the Office of Science for the Office of Isotope R&D and Production. This work was supported by the Laboratory Directed Research and Development Program of Oak Ridge National

Laboratory, managed by UT-Battelle, LLC, for the U.S. Department of Energy under contract DE-AC-05-000R22725.

Author Contributions

Conceptualization (H.B.A.), Data curation (H.B.A., Z.B.K., B.T.M.), Formal analysis (H.B.A.,), Funding acquisition (H.B.A., J.M.), Investigation (H.B.A., Z.B.K.), Methodology (H.B.A., Z.B.M., L.R.S.), Visualization (H.B.A.), Writing - original draft (H.B.A.), Writing - review & editing (all authors)

References

1. E. González-Roubaud, D. Pérez-Osorio, C. Prieto. “Review of commercial thermal energy storage in concentrated solar power plants: Steam vs. molten salts”. Renewable and sustainable energy reviews. 2017. 80: 133-148.
2. H. Moriyama, A. Sagara, S. Tanaka, R. Moir, D. Sze. “Molten salts in fusion nuclear technology”. Fusion Engineering and design. 1998. 39: 627-637.
3. J. Serp, M. Allibert, O. Beneš, S. Delpech, O. Feynberg, V. Ghetta, D. Heuer, D. Holcomb, V. Ignatiev, J.L. Kloosterman. “The molten salt reactor (MSR) in generation IV: overview and perspectives”. Progress in Nuclear Energy. 2014. 77: 308-319.
4. M. Stoddard, J. Harb, M. Memmott. “Numerical analysis of isotope production in molten salt reactors: A case study for Molybdenum-99 production”. Annals of Nuclear Energy. 2019. 129: 56-61.
5. J. Moon, K. Myhre, H. Andrews, J. McFarlane. “Molybdenum-99 from Molten Salt Reactor as a Source of Technetium-99 m for Nuclear Medicine: Past, Current, and Future of Molybdenum-99”. Nuclear Technology. 2023. 209(6): 787-808.
6. A. Ho, M. Memmott, J. Hedengren, K.M. Powell. “Exploring the benefits of molten salt reactors: An analysis of flexibility and safety features using dynamic simulation”. Digital Chemical Engineering. 2023. 7: 100091.
7. S.E. Skutnik, P.W. Sobel, M.W. Swinney, K.K. Hogue, M.M. Arno, S.S. Chirayath. “Survey of prospective techniques for molten salt reactor feed monitoring”. Annals of Nuclear Energy. 2024. 208: 110796.
8. A. Danon, O. Muránsky, I. Karatchevtseva, Z. Zhang, Z. Li, N. Scales, J. Kruzic, L. Edwards. “Molten salt corrosion (FLiNaK) of a Ni–Mo–Cr alloy and its welds for application in energy-generation and energy-storage systems”. Corrosion Science. 2020. 164: 108306.
9. S. Guillot, A. Faik, A. Rakhmatullin, J. Lambert, E. Veron, P. Echegut, C. Bessada, N. Calvet, X. Py. “Corrosion effects between molten salts and thermal storage material for concentrated solar power plants”. Applied Energy. 2012. 94: 174-181.
10. K. Sridharan, T. Allen. “Corrosion in molten salts”. In: Molten salts chemistry. Elsevier, 2013. Pp. 241-267.

11. J.Y. Lim, J. Li, D. O'Grady, T. Downar, K. Duraisamy. "A hybrid surrogate modeling framework for the Digital Twin of a Fluoride-salt-cooled High-temperature Reactor (FHR)". Nuclear Engineering and Design. 2025. 433: 113690.
12. C. Guerrieri, A. Cammi, L. Luzzi. "An approach to the MSR dynamics and stability analysis". Progress in Nuclear Energy. 2013. 67: 56-73.
13. S.D. Branch, H.M. Felmy, A. Schafer Medina, S.A. Bryan, A.M. Lines. "Exploring the complex chemistry of uranium within molten chloride salts". Industrial & Engineering Chemistry Research. 2023. 62(37): 14901-14909.
14. W.B. Derdeyn, S. Mastromarino, R. Gakhar, M.H. Anderson, M.A. Kats, R.O. Scarlat. "Optical spectroscopy of molten fluorides: Methods, electronic and vibrational data, structural interpretation, and relevance to radiative heat transfer". Journal of Molecular Liquids. 2023. 385: 121936.
15. L.M. Toth, J.P. Young, G.P. Smith. "Diamond-windowed cell for spectrophotometry of molten fluoride salts". Analytical Chemistry. 1969. 41(4): 683-685.
16. J. Young. "Windowless Spectrophotometric Cell for Use with Corrosive Liquids". Analytical Chemistry. 1964. 36(2): 390-392.
17. J. Young, J. White. "High-temperature cell assembly for spectrophotometric studies of molten fluoride salts". Analytical Chemistry. 1959. 31(11): 1892-1895.
18. A.S. Medina, H.M. Felmy, M.E. Vitale-Sullivan, H.E. Lackey, S.D. Branch, S.A. Bryan, A.M. Lines. "Iodine and carbonate species monitoring in molten NaOH–KOH eutectic scrubber via dual-phase in situ Raman spectroscopy". ACS omega. 2022. 7(44): 40456-40465.
19. A. Weisberg, R.E. Lakis, M.F. Simpson, L. Horowitz, J. Craparo. "Measuring lanthanide concentrations in molten salt using laser-induced breakdown spectroscopy (LIBS)". Applied spectroscopy. 2014. 68(9): 937-948.
20. C. Hanson, S. Phongikaroon, J.R. Scott. "Temperature effect on laser-induced breakdown spectroscopy spectra of molten and solid salts". Spectrochimica Acta Part B: Atomic Spectroscopy. 2014. 97: 79-85.
21. Y. Lee, R.I. Foster, H. Kim, S. Choi. "Machine learning-assisted laser-induced breakdown spectroscopy for monitoring molten salt compositions of small modular reactor fuel under varying laser focus positions". Analytica Chimica Acta. 2023. 1241: 340804.
22. Y. Lee, S. Yoon, N. Kim, D. Kang, H. Kim, W. Yang, M. Burger, I. Jovanovic, S. Choi. "In-situ measurement of Ce concentration in high-temperature molten salts using acoustic-assisted laser-induced breakdown spectroscopy with gas protective layer". Nuclear Engineering and Technology. 2022. 54(12): 4431-4440.
23. A. Williams, S. Phongikaroon. "Laser-induced breakdown spectroscopy (LIBS) measurement of uranium in molten salt". Applied spectroscopy. 2018. 72(7): 1029-1039.
24. H.B. Andrews, Z.B. Kitzhaber, D. Orea, J. McFarlane. "Real-time elemental and isotopic measurements of molten salt systems through laser-induced breakdown spectroscopy". Journal of the American Chemical Society. 2024. 147(1): 910-917.
25. Z.B. Kitzhaber, D. Orea, J. McFarlane, B.T. Manard, H.B. Andrews. "Sparge Sampling of Molten Salts for Online Monitoring via Laser-Induced Breakdown Spectroscopy". ACS Omega. 2025. 10(33): 37889-37897.
26. E.H. Kwapis, J. Borrero, K.S. Latty, H.B. Andrews, S.S. Phongikaroon, K.C. Hartig. "Laser ablation plasmas and spectroscopy for nuclear applications". Applied spectroscopy. 2024. 78(1): 9-55.

27. A.M. Lines, G.B. Hall, S. Asmussen, J. Allred, S. Sinkov, F. Heller, N. Gallagher, G.J. Lumetta, S.A. Bryan. “Sensor fusion: comprehensive real-time, on-line monitoring for process control via visible, near-infrared, and Raman spectroscopy”. Acs Sensors. 2020. 5(8): 2467-2475.
28. L.R. Sadergaski, H.B. Andrews, B.A. Wilson. “Comparing sensor fusion and multimodal chemometric models for monitoring U (VI) in complex environments representative of irradiated nuclear fuel”. Analytical Chemistry. 2024. 96(4): 1759-1766.
29. G. LeCroy, Q. Yang, M. Raab, R. Gakhar, A. Williams. “Online monitoring of Lanthanide species with combined spectroscopy in flowing aqueous aerosol systems”. 2025.
30. K. Keerthi, S.D. George, S.D. Kulkarni, S. Chidangil, V. Unnikrishnan. “Elemental analysis of liquid samples by laser induced breakdown spectroscopy (LIBS): Challenges and potential experimental strategies”. Optics & Laser Technology. 2022. 147: 107622.
31. H.B. Andrews, K.G. Myhre. “Quantification of lanthanides in a molten salt reactor surrogate off-gas stream using laser-induced breakdown spectroscopy”. Applied spectroscopy. 2022. 76(8): 877-886.
32. G. Lothian. “Beer's law and its use in analysis. A review”. Analyst. 1963. 88(1050): 678-685.
33. H.B. Andrews, L.R. Sadergaski. “Leveraging visible and near-infrared spectroelectrochemistry to calibrate a robust model for Vanadium (IV/V) in varying nitric acid and temperature levels”. Talanta. 2023. 259: 124554.
34. J.-M. Mermet. “Limit of quantitation in atomic spectrometry: An unambiguous concept?”. Spectrochimica Acta Part B: Atomic Spectroscopy. 2008. 63(2): 166-182.

Supporting Information

Design of Molten Salt Flow Cell for Combined Laser-Induced Breakdown Spectroscopy and Absorbance Spectroscopy Online Measurements

Hunter B. Andrews,[1,*] Zechariah B. Kitzhaber,[1] Daniel Orea,[2] Luke R. Sadergaski,[1] Benjamin T. Manard,[3] Kevin Robb,[2] Joanna McFarlane[2]

Fig. S1. Photograph of sample stream passing through SCORCH cell.

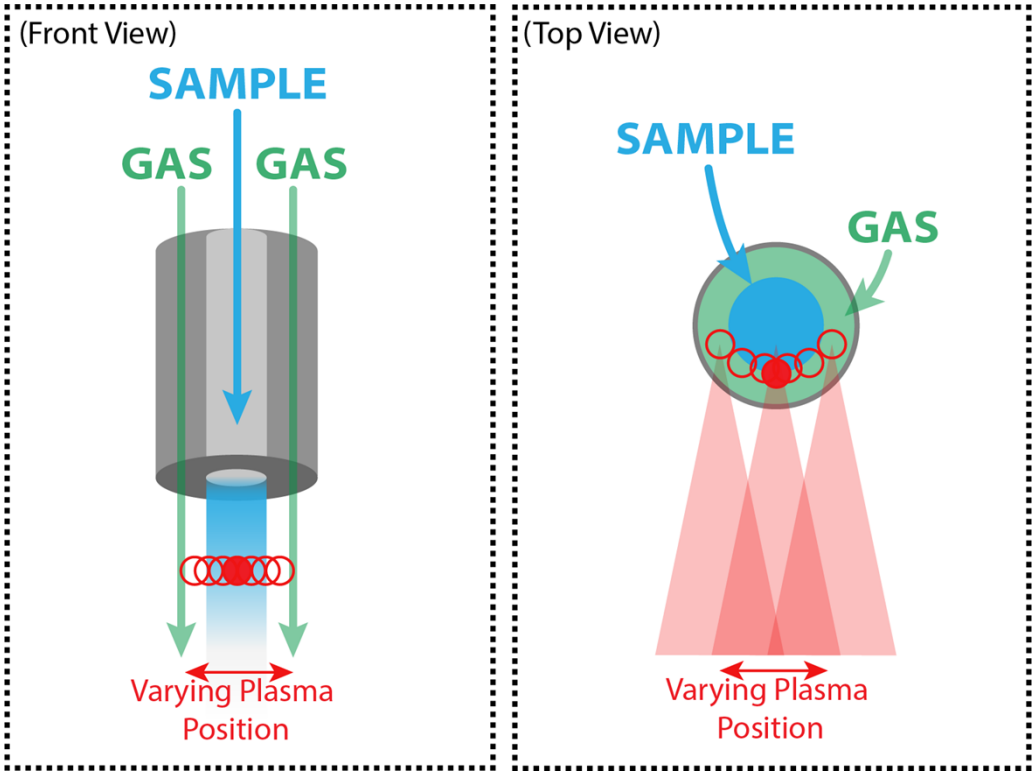

Fig. S2. Graphic illustrating how the plasma position tests were completed.

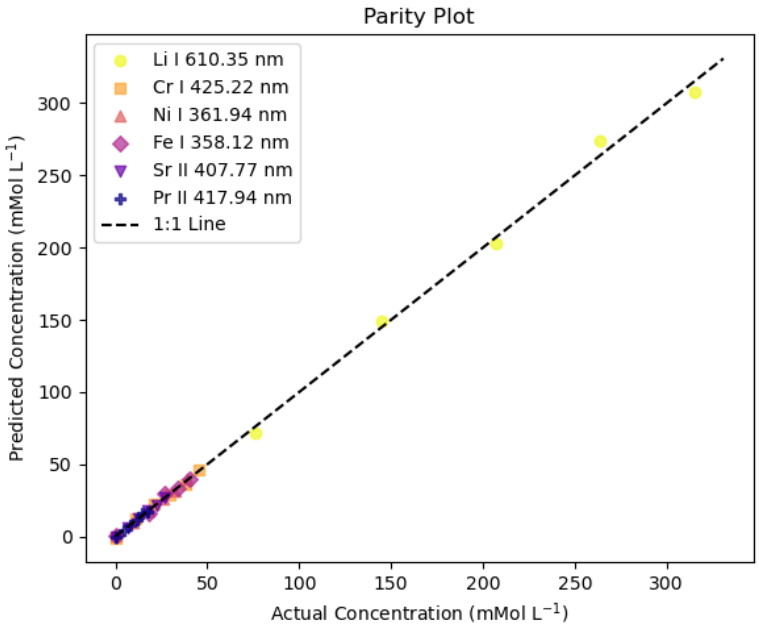

Fig. S3. Parity plot of LIBS model predictions during cross validation. The dashed 1:1 line represents a perfect prediction.

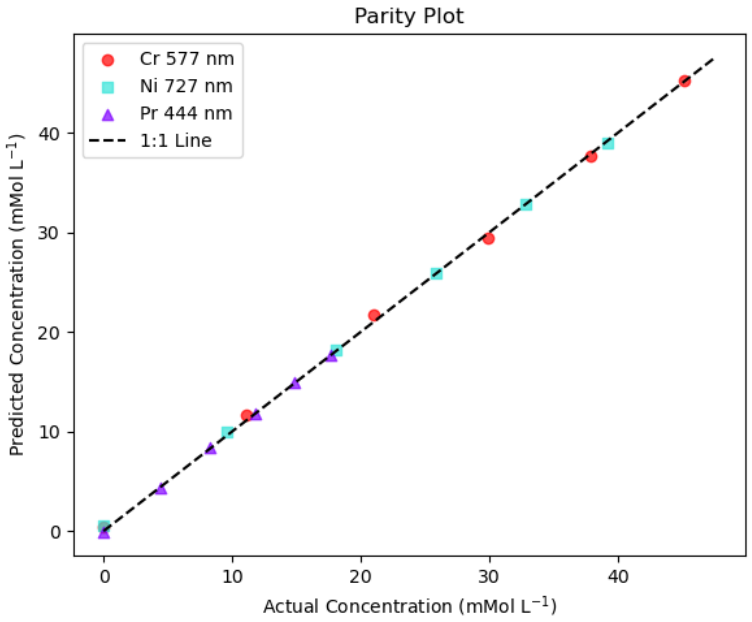

Fig. S4. Parity plot of absorbance model predictions during cross validation. The dashed 1:1 line represents a perfect prediction.